CrossMark

Photocatalytic and antibacterial studies of indium-doped ZnO nanoparticles synthesized by co-precipitation technique

K. Pradeev Raj[1,2] · K. Sadaiyandi[3] · A. Kennedy[2] · Suresh Sagadevan[4]

Abstract   Indium (0.01, 0.04 and 0.06 mol%) doped ZnO nanoparticles (IZ-NPs) have been synthesized using the facile co-precipitation method. The prepared nanoparticles (NPs) were characterized by X-ray diffraction (XRD), scanning electron microscopy (SEM), Elemental dispersive spectroscopy (EDS), UV–Vis absorption spectrum (UV–Vis) and photoluminescence (PL) techniques. The photocatalytic activities were evaluated for the degradation of Rhodamine-B (Rh-B) under UV–Vis irradiation. The antibacterial properties of Zinc oxide nanoparticles (NPs) were investigated using human pathogens and were compared based on the diameter of inhibition zone using Agar-well diffusion method. Structural studies confirm the main presence of hexagonal wurtzite ZnO phase and well-crystalline. The incorporation of indium ions was responsible for the change in their various lattice parameters. The average crystallite sizes were decreased by increasing the indium dopant concentration. SEM images reveal the synthesized NPs are in nanometer range with various shape and improved crystallinity is noted for higher doping (In) concentration. The presence of indium in the host lattice was confirmed by EDS spectroscopy. Optical studies shows that the band-gap energy decreases (3.34–3.17) with an increase in doping concentration (2–6%). The photoluminescence (PL) spectrum reveals the UV emission is strong near the band-edge region (NBE) (392 nm) and intrinsic defects encountered in series of visible emission peaks around 400–560 nm. From the efficiency of the photocatalytic activity, higher dopant concentration (6%) showed higher photocatalytic activity than the other NPs in destroying Rhodamine B (RhB) under UV–Vis light irradiation. The synthesized In-doped Zinc oxide nanostructures show maximum antibacterial activity against *Staphylococcus aureus* and *Staphylococcus epidermidis*.

1 Introduction

Nanoscale materials and nanotechnology have attracted huge attention in recent years. ZnO is one of the most promising semiconductor materials, which has fascinated much attention owing to a wide range of applications in the field of science and technology. Because of its wide and direct band gap (3.37 eV) equivalent that of GaN [1], ZnO has drawn much interest in the field of Optoelectronic devices [2], potential candidate for solar energy conversion [3], storage devices [4], luminescence [5], transparent UV protection films, chemical sensors, spintronic devices [6], antibacterial agent, [7], gas sensing [8] and an excellent photocatalysts [9] etc. Further, ZnO nanostructures have a high redox potential, excellent physical and chemical stability, inexpensive, easy synthesis and non-toxic [10].

In the ground of photocatalysis presently ZnO doped with appropriate metals has emerged as the leading material in the green environment. When comparing with TiO$_2$ nanoparticles for the degradation of dyes, ZnO confirms to be an enhanced photocatalyst due to its high efficiency and mobility of photo-induced charge carriers [11]. The greatest

✉ Suresh Sagadevan
drsureshnano@gmail.com

1   Research and Development Centre, Bharathiar University, Coimbatore, Tamil Nadu 641 046, India

2   Department of Physics, CSI College of Engineering, Ooty, Tamil Nadu 643 215, India

3   Department of Physics, Alagappa Government Arts College, Sivagangai, Karaikudi, Tamil Nadu 630 003, India

4   Centre for Nanotechnology, AMET University, Chennai 603 112, India

advantage of ZnO is the ability to absorb a wide range of solar spectrum and more light quanta than some other semiconducting metal oxides [12]. ZnO has the hexagonal close packed lattice with empty octahedral sites. In this connection, Zinc oxide has a high surface reactivity because of a large number of native defect sites [13]. From the literature, it is evident that doping with suitable cations or anions with ZnO in the degradation of various dyes has been drastically improved its photocatalytic activity and to further widen its light absorption in the visible region [14]. The incorporation of alkali metal ions into the ZnO matrix results in the formation of significant lattice defects, that may be attributed to the charge compensation and ionic radius mismatch between Zinc and the corresponding dopant [15].

When the cationic dopant is added to ZnO, the photodegradation efficiency of ZnO is improved further. Several locations are possible for the cationic dopant deposition which results on the surface, Zn sites within the lattice of ZnO crystal and the interstitial sites of the ZnO matrix [16]. Adding doping element could also reduce the activation energy in the photocatalytic mechanism. Further, ZnO exhibits high reaction and mineralization rates [17] which can trigger more hydroxyl ions with comparing to than other metal oxides [18]. Thus, the incorporated dopants act as electron traps, which suppress the recombination of photo-generated holes and electrons [19] that could enhance the photocatalytic activity in the visible region under the entire spectrum of sunlight. Further, Toxicity studies have shown that zinc ions do not cause any harms to the DNA of human cells [20]. Bacteria's, such as *Staphylococcus epidermis, Staphylococcus aureus, Pseudomonas* sp. and *Escherichia coli* have the ability to cause localized skin contagion, diffuse skin infection, necrotizing Pneumonia, urinary tract infection (UTI) and respiratory infections. These infections are wide spreading nowadays and it is difficult to recognize. With the increase in urbanization, migration, and settlement, people are exposed to more airborne, vector-borne and zoonotic spread of infectious agents [21]. Therefore, in terms of potential use, the incorporation of nano metal oxides into surfaces and other objects could be studied in order to reduce some of the infectious diseases. Among the various metal oxides nanoparticles, doped ZnO nanoparticles play a pivotal role in acting as an antibacterial agent against bacteria. Several techniques have been adopted to synthesise pure and doped ZnO NPs like the vapour transport process [22] spray pyrolysis [23], thermal decomposition [24], hydrothermal method [25], sol–gel method [26], hydrolysis, [27], chemical precipitation [28], electrochemical method [29] in order to tailor its morphology and size. Among them, the standard co-precipitation method is simple, inexpensive and mass production at room temperature to synthesize pure and doped ZnO NPs [30]. In our previous work, we have studied the structural, optical, photoluminescence and photocatalytic assessment of Sr-doped ZnO Nanoparticles [31].

In this present study, a special emphasis is taken to study the Antibacterial activity along with the Photocatalytic studies between pure and Indium doped ZnO NPs prepared via co-precipitation technique. However, it is noteworthy to mention that both pure and In-doped ZnO NPs were synthesized on a high altitude region (>2200 m above sea level, Ketti, The Nilgiris, Tamil Nadu, India) at a room temperature of 18 °C as previously reported in our earlier work [29] and now the same method is employed to dope Indium with various concentrations. Samples were characterized using X-ray diffraction (XRD), scanning electron microscope (SEM), photoluminescence emission spectra (PL), UV–Vis spectrophotometer. Photodegradation studies on Rhodamine B dye (RhB) at various intervals (0–120 min) were carried under UV–Visible irradiations. The antibacterial activity for pure and Indium doped ZnO nano structures towards *S. aureus* and *S. epidermis* was tested by an agar disc diffusion method.

2 Materials and methods

Pure and In-doped ZnO NPs was achieved by simple co-precipitation method. An appropriate quantity of Zinc chloride ($ZnCl_2$) and Sodium hydroxide (NaOH) were mixed with deionized water in the molar volume of 1:1. The main role of sodium hydroxide during the synthesis is used to precipitate the transition metal hydroxides. It acts as a specific intermediate in accelerating the reduction and increasing the rate of formation of ZnO and In–ZnO nanoparticles. Further, sodium hydroxide is used for converting $ZnCl_2$ to $Zn(OH)_2$ which on heating gives water to form ZnO nanoparticles. A buffer solution of 1 M of sodium carbonate (Na_2CO_3) is taken separately in another beaker. Further, the buffer solution is added dropwise to the in initial solution under constant stirring for 5 h at room temperature to obtain a white precipitate. The reaction was stopped and sufficient time was given for the entire precipitation to settle at the bottom. This precipitate was then allowed for complete settlement for 12 h at a room temperature. The final product was washed several times and then dried in a hot air oven at 100 °C to remove water molecules. Finally, the synthesized nanoparticles (NPs) were calcined at 600 °C for 4 h and then, crushed into fine ZnO NPs. same process was adopted to synthesize In-doped ZnO NPs. Different concentrations of Indium Chloride $InCl_2$ (0.02, 0.04, 0.06 M) was added to an appropriate quantity of distilled water and (0.98, 0.96, 0.94 mol%) Zinc Chloride $ZnCl_2$ were added into the appropriate amount of distilled water and the same procedure remains as of pure ZnO NPs as said above.

The structural and phase characterization was carried by X-ray diffraction (XRD) studies, Surface morphology is done using the Scanning Electron Microscope (SEM). Optical studies were carried at room temperature using a UV–Vis (Perkin Elmer) spectrophotometer and Photoluminescence (PL) emission studies were carried by (JobHR800 in Yoon Horbe) spectrometer using a He–Cd laser source with a wavelength of 325 nm.

2.1 Measurement of photocatalytic activity

Experiments were performed in a quartz reactor of 150 ml capacity, provided with water circulation in order to maintain a constant temperature. The UV irradiation was carried out by using 125 W (311 nm) medium pressure Hg arc lamp (SAIC, INDIA). 150 ml of desired initial concentration (20 ppm) of RhB dye solution was mixed with a fixed amount ZnO NPs (50 mg) at natural pH (6.2). This mixture is then magnetically stirred and subjected to UV illumination. The sample from the photoreactor is withdrawn at different time intervals and centrifuged. The supernatants are analyzed for its absorption maximum (585 nm) using UV–Vis Spectrophotometer. Similar procedure was adopted for the incorporation of various concentrations In dopants (2, 4 and 6%) into RhB dye solution. Percentage of RhB absorbed on the catalyst surface was calculated from the following equation.

Percentage of degradation $= (C_0 - C_t)/C_0 \times 100\%$

where C_0 represents the initial time in absorption and C_t represents the absorption after' minutes.

The total organic carbon (TOC) for all the samples were analyzed by direct inoculation of the filtered sample solutions into a Thermo Euroglas, Model TOC 1200, total organic carbon analyzer (Thermo Electron Corporation, The Netherlands).

2.2 Antibacterial activity

The antibacterial activity of the synthesized samples was tested towards *S. aureus* and *S. epidermidis* was performed by an agar disc diffusion technique. The bacterial suspension was applied uniformly on the surface of nutrient agar medium (NAM) plate and agar-wells were punched using agar punches. Then, the synthesized nanoparticles were added in the 0.1%/l concentration. The plates were incubated at 37 °C for 24 h, after which the average diameter of the inhibition zone surrounding the disk was measured with a ruler up to 1 mm resolution.

3 Results and discussion

3.1 Structural studies

The XRD diffraction pattern for pure and In-doped ZnO NPs are shown in Fig. 1. It is noted from Fig. 1, the diffraction peaks corresponding to (100), (002), (101), (102), (110), (103) and (112) are with a hexagonal phase ZnO of Wurtzite structure (JCPDS 36-1451, space group $p6_3mc$) [32]. It is noted that no other peaks were observed confirming the purity and the crystalline nature of the synthesized NPs. It is interesting to observe there is a negligible peak shift towards the lower diffraction angle occurred as a result of In doping into ZnO matrix. This may be attributed due to the lattice strain occurred as a result of In doping into ZnO lattice [33].

The crystalline size (D) is calculated by using the Debye–Scherrer's formula as given below [34]

$$D = 0.9\lambda/\beta \cos\theta \qquad (1)$$

where λ is the X-ray wavelength of 1.54 Å, β is the full-width half maximum, θ is the Bragg's diffraction angle. The average crystallite size and is listed in Table 2. From the calculated values it is found the crystallite size decreased with the increase of In content. This may be due to the reduction in diffusion rate which makes the NPs intact and due to the distortion in the host ZnO lattice by foreign impurities [35].

3.2 Effect of doping on lattice parameters

The physical properties of the pure and In-doped ZnO NPs are strongly affected by various parameters such as crystallite size, dislocation density, bond length and lattice strain [36]. In the case of wurtzite phase, the lattice parameters are calculated by using the formula Eqs. (3–5)
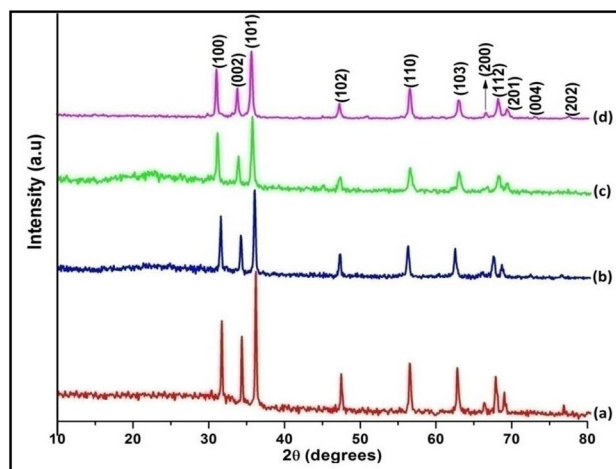
Fig. 1 XRD pattern for pure and IZ-ZnO NPs: *a* Pure ZnO NPs, *b* 2% IZ-NPs, *c* 4% IZ-NPs, *d* 6% IZ-NPs

$$\frac{1}{d_{hkl}} = \frac{(h^2 + k^2)}{a^2} + \frac{l^2}{c^2} \tag{2}$$

$$a = \frac{\lambda}{\sqrt{3}\sin\theta_{100}} \tag{3}$$

$$E = \frac{\left[h^2 + \frac{(h+2k)^2}{3} + \left(\frac{al}{c}\right)^2\right]^2}{S_{11} + \left(h^2 + \frac{(h+2k)^2}{3}\right)^2 + S_{33}\left(\frac{al}{c}\right)^4 + (2S_{13} + S_{44})\,h^2 + \frac{(h+2k)^2}{3}\left(\frac{al}{c}\right)^2} \tag{7}$$

$$c = \frac{\lambda}{\sin\theta_{002}} \tag{4}$$

where $a = b$ and c are the lattice parameters, d_{hkl} is the interplanar distance corresponding to its Miller indices (hkl). The calculated lattice parameters are presented in Table. From Table 1 it is noted that there is a small change in its lattice parameters; this may due to the change in its crystallite size and difference in their atomic radius with respect to their doping concentration [37].

Dislocation density (δ), which represents the amount of defect present in the sample and is calculated using Eq. (5) [38],

$$\delta = \frac{1}{D^2} \tag{5}$$

From Table 2, it is observed that the dislocation density is slightly increased with doping. This may be due to the decrease in grain size and the presence of defect states [39].

Strain induced is calculated using the Eq. (6)

$$\varepsilon = \beta_{hkl}\cos\theta/4 \tag{6}$$

It is noted from Table 2, there is an increase in its lattice stress and strain as a result of In ions doped into ZnO environment.

Young's modulus (E) for a hexagonal wurtzite structure is given by the following relation.

where S_{11} (7.86×10^{-12} m^2 N^{-1}), S_{13} (-2.206×10^{-12} m^2 N^{-1}), S_{33} (6.940×10^{-12} m^2 N^{-1}) and S_{44} (23.57×10^{-12} m^2 N^{-1}) are the elastic coefficient of ZnO [40]. From Table 2, the calculated value of Young's modulus is found to be constant for both pure and IZ-NPs. This indicates the doping concentration do not have any significant effect on Young's Modulus (E). Similar results were obtained by Yousefi et al. in investigating the properties of Mg-doped ZnO nanoparticles [41]. Also for an elastic system, the energy density (u) per unit lattice is calculated by the following Eq. (8) [42].

$$u = \frac{E_{hkl}\varepsilon^2}{2} \tag{8}$$

It is observed that the energy density has found to increase with In doping concentration. This is because energy states increase with doping concentration. Thus doping plays a vital role in changing the physical property of the material [43].

Table 1 Lattice parameters of pure and IZ-NPs

Sample	Lattice parameter			Atomic packing fraction (APF) %	Volume (nm^3)
	a (Å)	c (Å)	c/a ratio		
Pure ZnO NPs	3.25	5.21	1.6004	75.42	47.19
2% IZ-NPs	3.24	5.19	1.6012	75.44	47.35
4% IZ-NPs	3.24	5.19	1.6019	75.44	47.59
6% IZ-NPs	3.25	5.20	1.6035	75.51	47.81

Table 2 Geometric parameters of pure and IZ-NPs

Sample	Crystal size (D) nm	Micro strain (no unit)	Stress σ (MPa)	Dislocation density (δ) (K J m^{-3})	Young's modulus (E) (GPa)	Energy/unit lattice (U) K J m^{-3}
ZnO NPs	50.2	7.197×10^{-4}	0.1036	3.97×10^{-4}	144	37.3
2% IZ-NPs	40.1	9.375×10^{-4}	0.1351	6.22×10^{-4}	144	63.3
4% IZ-NPs	32.5	1.594×10^{-3}	0.1820	9.48×10^{-4}	144	115.1
6% IZ-NPs	28.4	1.263×10^{-3}	0.2293	1.24×10^{-3}	144	183.2

4 SEM analysis

Figure 2a–d shows the SEM images of pure and IZ-NPs. From the figure, it is noted that the surface of the synthesized NPs exhibits shapes like hexagon, cube, polygon and rod-shaped nanostructures. It is also observed that a uniform distribution of crystals throughout the surface without any cluster formation. Further, the crystallite size decreases (66.4–32.6 nm) with an increase in Indium concentration (2–6%). This inference on the decrement of the crystallite size with dopant concentration is consistent with the present XRD results.

The composition analyses of the samples are further quantitatively evaluated using energy dispersive X-ray spectroscopy (EDS) studies. Figure 3 shows the EDS spectra of Indium doped ZnO nanoparticles. The spectra indicate the occurrence of In, Zn, and O as the major elements along with the elemental chart. It is also observed from the obtained values of O (oxygen) content, the weight% of oxygen decrease with increase in indium doped NPs which confirms the substitution of Indium into ZnO matrix. No traces of other elements were found in the spectrum which confirms the purity of the samples.

5 Optical studies

Figure 4 shows the optical absorption and transmission spectra for pure and IZ-NPs. From the figure it is clear the optical absorption edge for pure and IZ-NPs is below 400 nm. It is also noted that for pure ZnO, high absorption owing in the UV region under 400 nm and slightly decreases with Indium dopant (In). This may be due to the incident photon having sufficient energy to interact with the atoms of the materials and therefore high absorption and low transmission occur in the UV-region [44]. As the doping of Indium increases (4–6%), it is interesting to see that there is a minor shift towards the longer wavelength region (Red shift) in the spectrum (Fig. 4a). This is due to the defects inducing a delocalization of the conduction band edge and creates deep traps in electronic energy states [45].
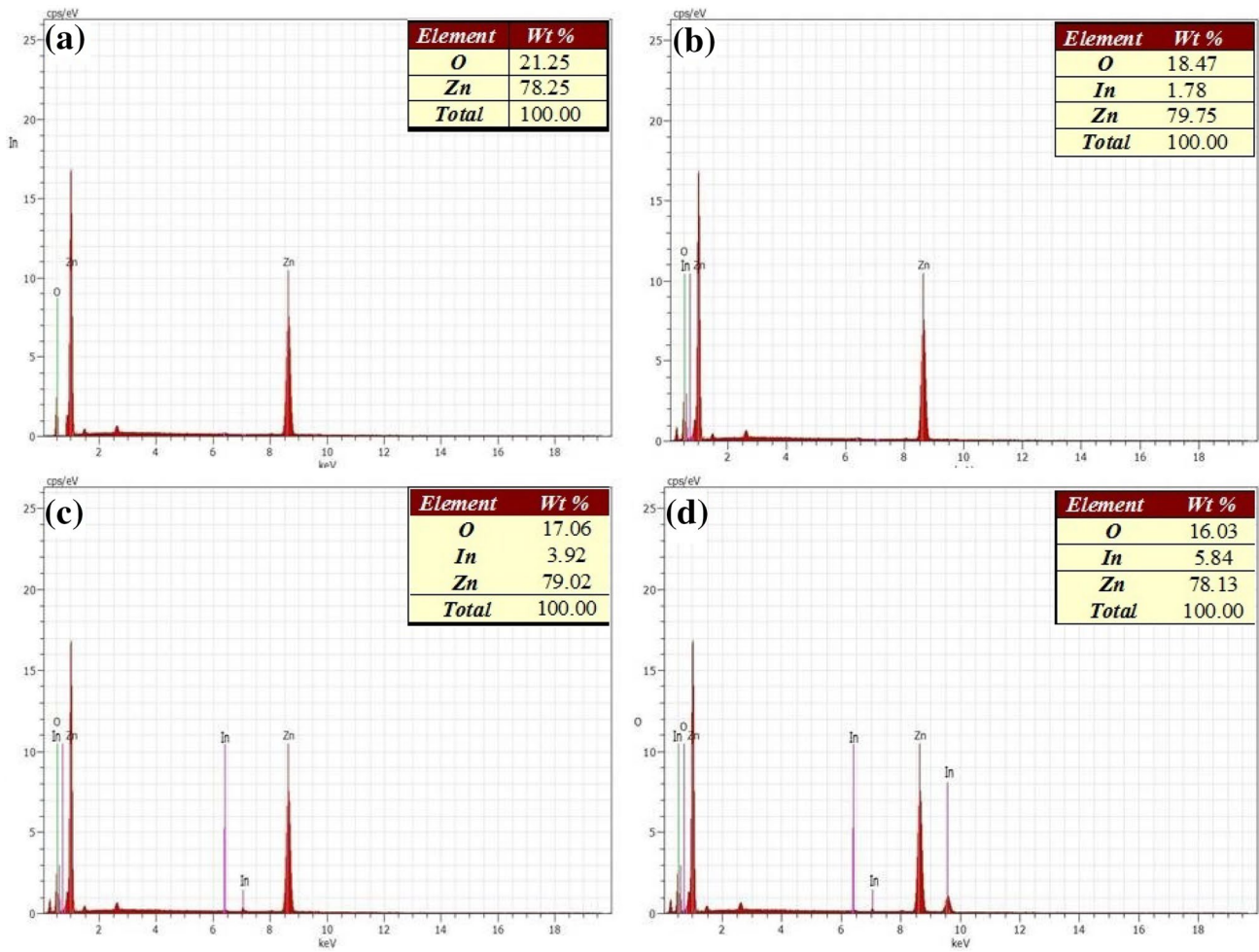
The optical band gap E_g is determined from a Tauc-plot from the following relation
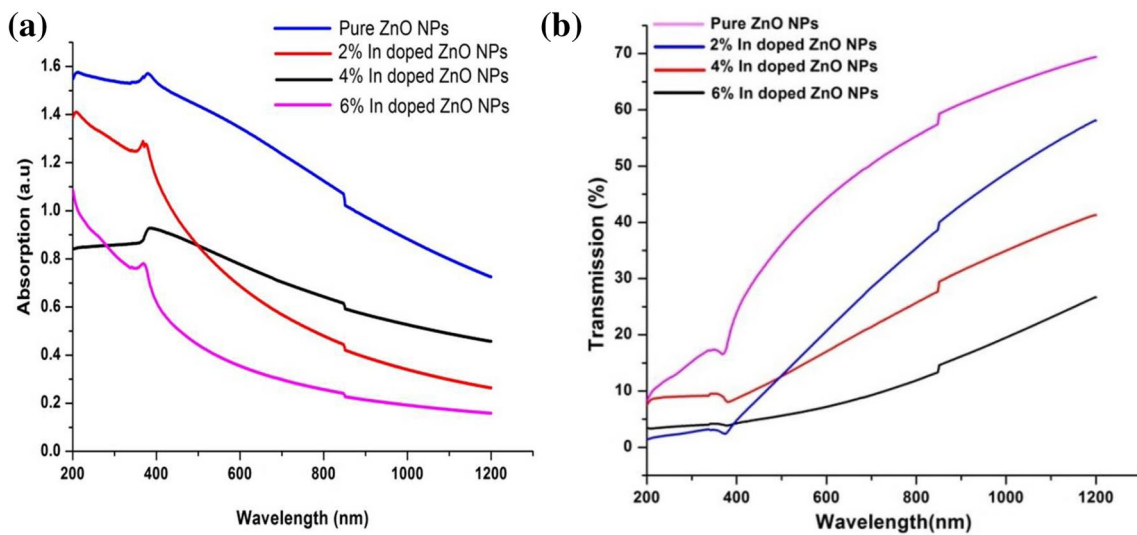
$$\alpha h\nu = A \left(h\nu - E_g\right)^n \tag{9}$$

where α is absorption coefficient, h is the Plank's constant, ν is the frequency of light radiation and E_g is the band gap energy where 'n' takes the value of 1/2 allowed direct
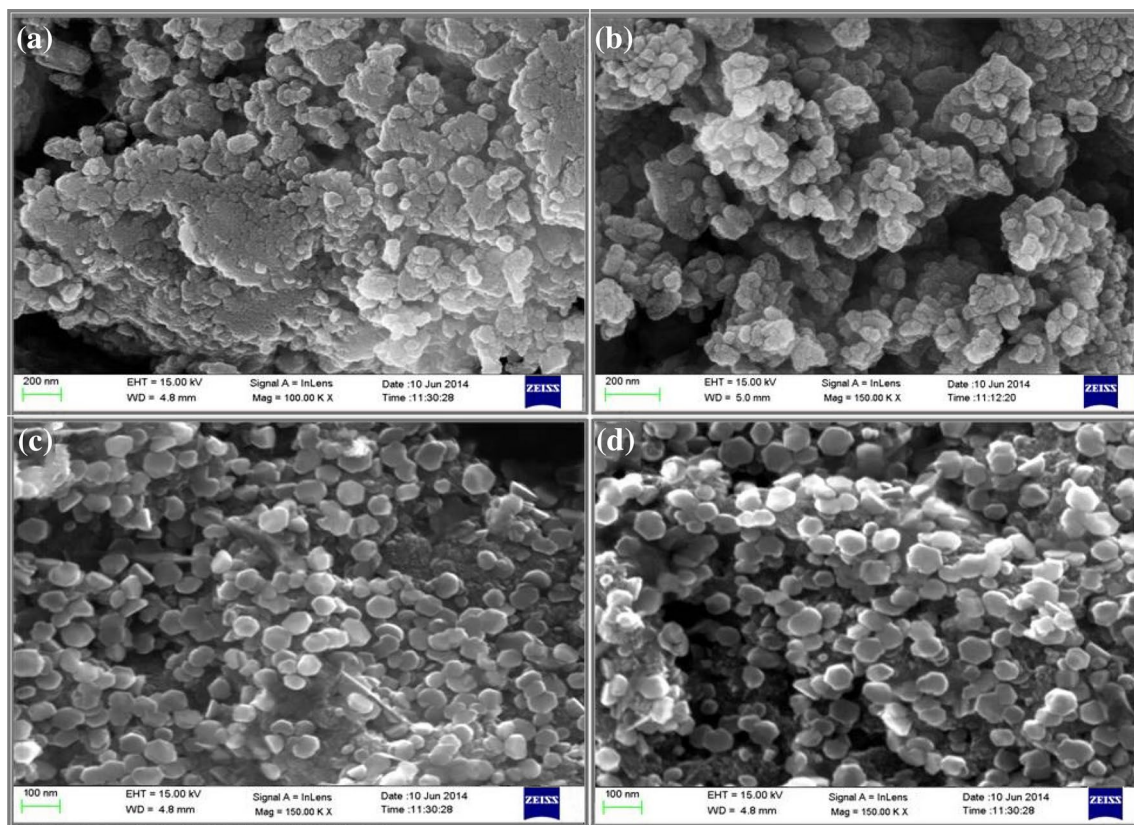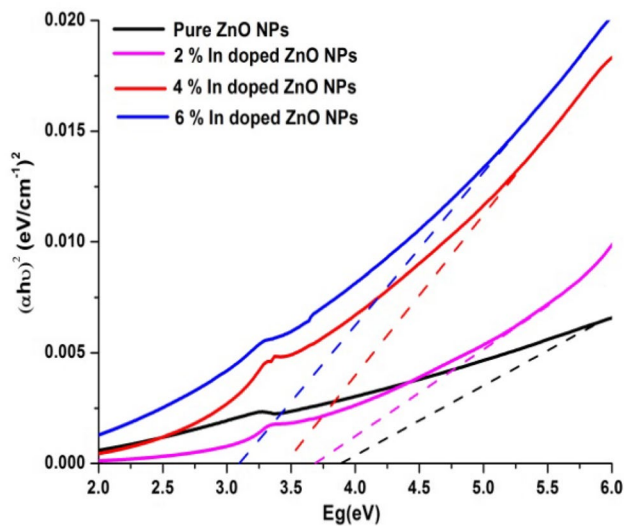

Fig. 2 SEM photographs of pure and In-doped ZnO NPs: **a** pure ZnO NPs, **b** 2% IZ-NPs, **c** 4% IZ-NPs, **d** 6% IZ-NPs

Fig. 3 Energy dispersive X-ray (EDX) spectra: **a** pure ZnO NPs, **b** 2% IZ-NPs, **c** 4% IZ-NPs, **d** 6% IZ-NPs

Fig. 4 Optical spectrum for pure ZnO and In-doped ZnO NPs: **a** absorption spectrum, **b** transmission spectrum
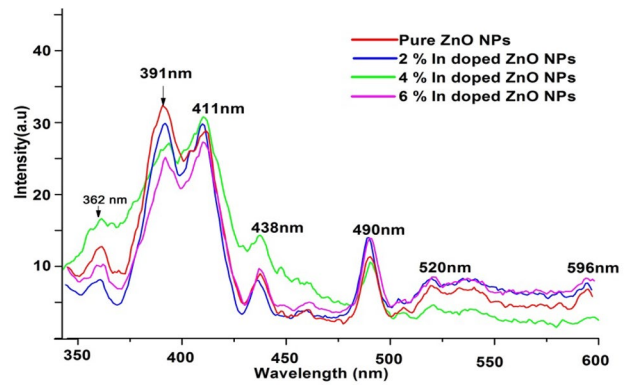
Fig. 5 Band gap energy (E_g) for pure and IZ-NPs

Fig. 6 Photoluminescence spectrum of pure and IZ-NPs

transition [46]. Plots of $(\alpha h\nu)^2$ and $(h\nu)$ are made for pure and In-doped ZnO NPs.

From the extrapolation of the linear portions of the plots onto the x-axis, E_g is found and the values are listed in Table 3. From Fig. 5, it is found that the band gap energy decreases with the increase of In doping concentration into ZnO matrix. The decrease in band gap perhaps due to the shallow level donor impurities creates additional energy levels in the bandgap near the conduction band edge [47]. A further change in lattice parameter from the ideal order and defects such as zinc excess or moderate oxygen vacancies can lead to a decrease in band gap energy values [48]. Moreover, the decrease in band-gap energy results in the increase in photon production and Photo-receptive [49]. Subsequently, it is accepted that IZ-4 should show a higher photocatalytic activity than other NPs.

6 Photoluminescence studies

PL Studies is an important tool to analyze defect states and their effects in optical studies. Figure 6 shows the PL spectra recorded at room temperature for pure and IZ-ZnO NPs at an excitation wavelength of 330 nm. It is observed from the figure, that several intense peaks are present in the wavelength region around 350–600 nm. Emission peaks at 362 and 391 nm originated in the UV-region. This may be due to the occurrence of free exciton-electron–hole recombination corresponding to the near band edge emission (NBE) during the impact process [50]. Further series of peaks at 411, 438, 490, 520 and 596 nm are observed in the wavelength range ranging from 400 to 600 nm (visible region).

It is interesting to note that the intensity of the peak in the visible spectral region (490 nm) slightly increases with the increase of dopant concentration (2–6%). This is due to the enhancement of more defect states such as the Zn vacancies, Interstitials, restrained oxygen vacancies and oxide antisite defect etc. [51]. It is well known that smaller sized nanoparticles have a higher population of surface defects for the enhanced defect emission relative to the UV–Vis emission, as seen in the presence of metal ion doped metal oxide nanoparticles [52]. Due to the increase in surface to volume ratio and concentration on oxygen vacancies, the grain size decreases it causes to the increase of the luminescence centers. In general, vacancies due to defects in doped ZnO NPs can act as the active centers to capture photo-induced electrons. This occurrence causes reduction of recombination, causing to higher photocatalytic activity.

7 Photocatalytic studies

The photocatalytic activity of IZ-NPs was investigated for Rhodamine-B dye under UV–Vis irradiation. Figure 7a–d shows the change in the optical absorption spectra of RhB dye solution for pure and In-doped ZnO NPs recorded at different intervals of time. From the Fig. 7 it is clear that the absorption decreases as the exposing time is increased from 0 to 120 min. It is interesting to note that from Fig. 7a only a negligible amount of degradation (8%) has occurred for pure ZnO NPs at 120 min in comparing to 6% IZ-NPs (Fig. 7d). Further, as the doping concentration increases enhancement in photodegradation is observed (Table 3). This may be due to the defect states and oxygen vacancies created for the while the doping content increased [53]. Figure 8a, b shows the Kinetics of RhB dye solution as a function of irradiation time. Where C is the concentration of RhB at its maximum absorption and C_0 is the initial absorption. It is observed from Fig. 8b the concentration of RhB decreases over a period of time as the In concentration is increased.
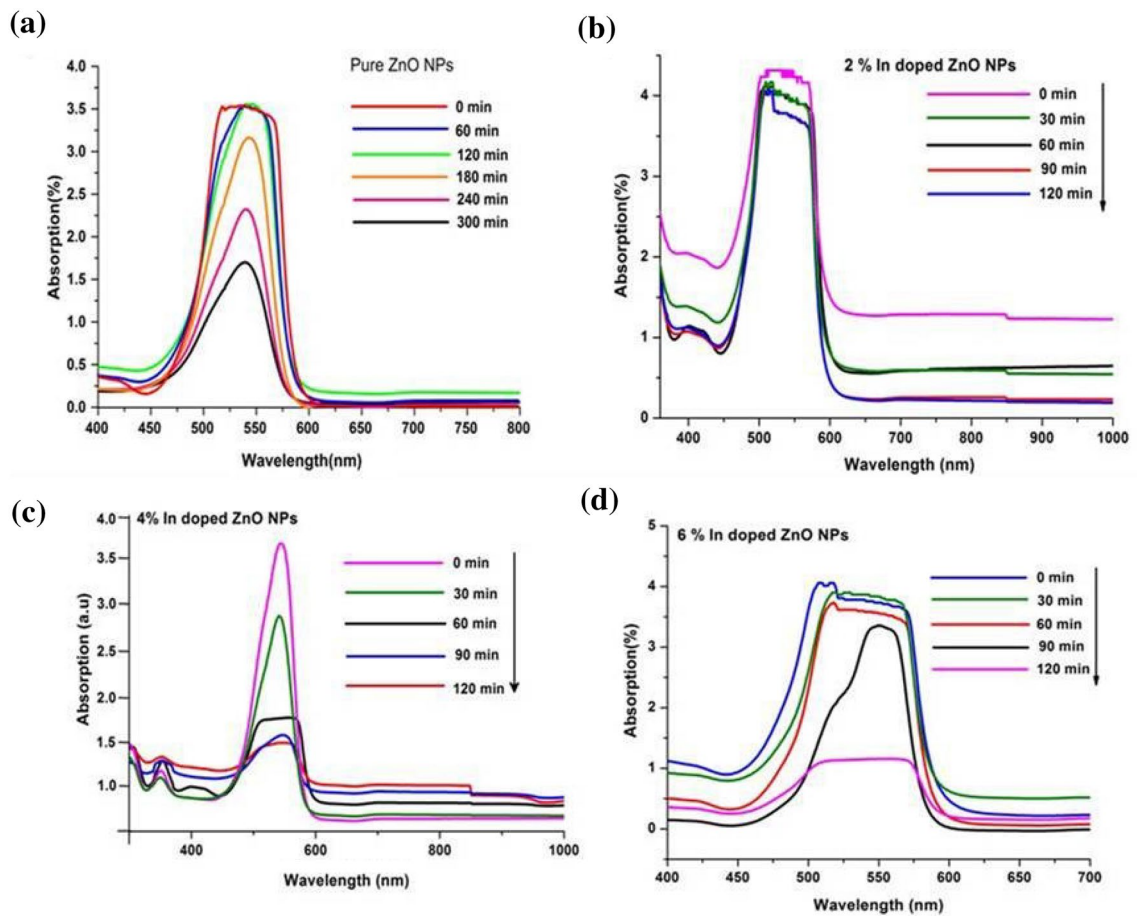
Fig. 7 a–d Absorption spectral decrement of Rhodamine B dye aqueous solution degraded from (0–120 min): **a** undoped ZnO, **b** 2% IZ-NPs, **c** 4% IZ-NPs, **d** 6% IZ-NPs
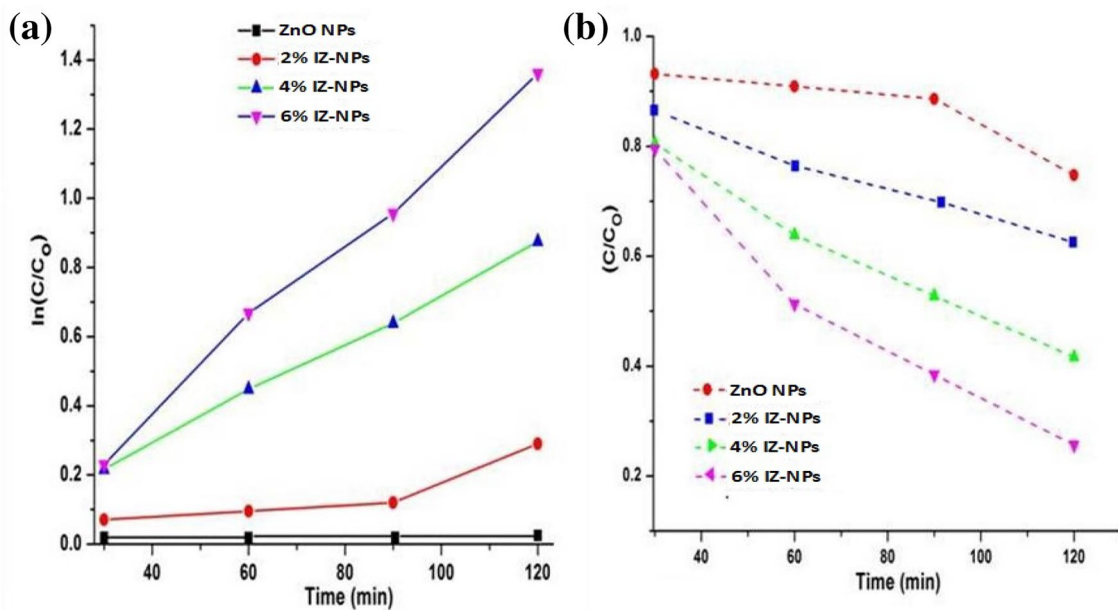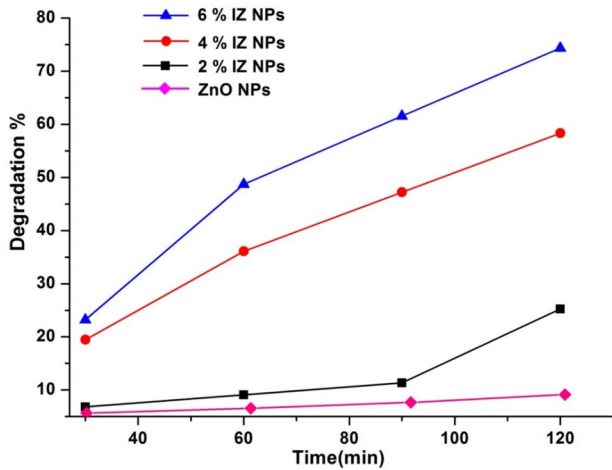

Fig. 8 Kinetics of RhB dye degradation for pure and IZ-NPs under UV–Visible radiations

Table 3 Photocatalytic degradation with band gap energy: (2–6% IZ-NPs)

Sample	Band gap (E_g)	Degradation (%) at 120 min	Degradation the rate constant (k)
ZnO	3.34	8	0.0002
2% IZ-NPs	3.28	25	0.0019
4% IZ-NPs	3.22	57	0.0072
6% IZ-NPs	3.17	76	0.0101

Fig. 9 Photodegradation of Rhodamine B under pure and IZ-NPs

The percentage of degradation of RhB from 0 to 120 m is shown in Fig. 9. It is noted for pure ZnO NPs only 8% of degradation has occurred for 120 min but for 2, 4 and 6% IZ-NPs the degradation is found to be 25, 57, and 76% respectively. This increase in its degradation is due to the fact that the active sites provided for the adsorption of the substrate on the catalyst surface are enhanced for IZ-NPs [54].

From the kinetics of degradation, the rate constant (k) for RhB is calculated by using the first order plot as given below

$$\ln\left(\frac{C_0}{C}\right) = kt \tag{10}$$

where C_0 and C are the reactant concentration at time t = 0 and t = t, correspondingly, k and t are the First-order rate constant and time. From the linear plot, the rate constant (k) for the degradation of RhB dye for pure and IZ-NPs are determined and summarized in Table 3.

From Table 3 it is observed that the degradation rate (k) increases with increase in doping concentration. High degradation rate constant demonstrates higher photocatalytic performance [55]. Thus the collective effects of the increased surface area and the small size nanoparticles induce better photocatalytic performance for the Indium-doped nanoparticles compared with pure ZnO NPs.

7.1 Mechanism of photocatalytic reaction

The mechanism of photocatalysis for In-doped ZnO NPs has been illustrated in Fig. 10a. Due to the decrease in activation energy, an increase in specific surface area by the incorporation of In dopant creates extra energy level, which can enhance the light absorption range and enhance the photoresponse of the cation (In) induced ZnO in the UV–Vis region [56].

The photocatalysis process is initiated by the generation of electron–hole pair irradiation. An electron from the valence band (VB) gets excited to the conduction band (CB) by absorbing UV light (h$\nu \geq E_g$), equal or greater than the band gap energy of ZnO (Eq. 11). This leads to
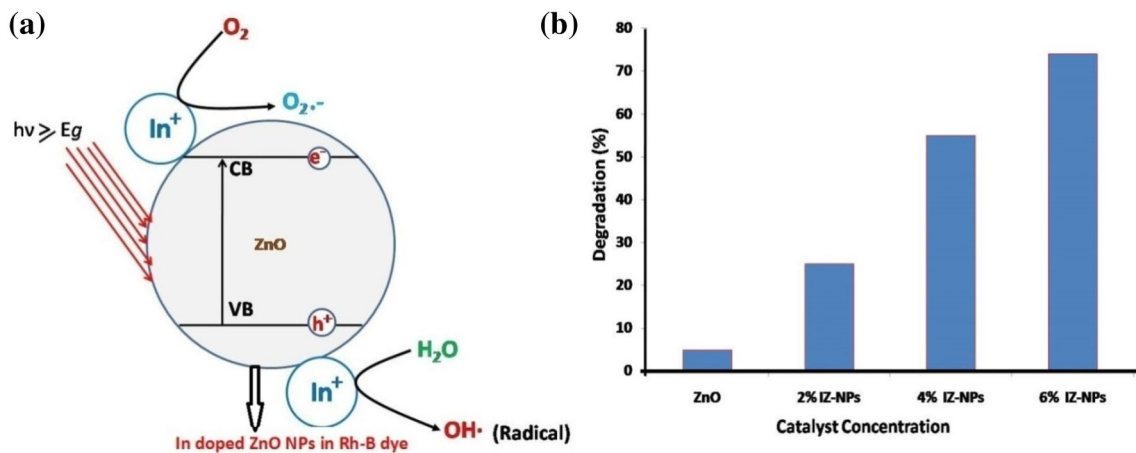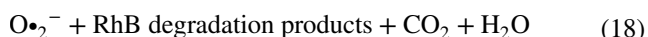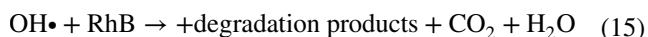

Fig. 10 **a** Photocatalytic degradation mechanism by In dopant on ZnO surface, **b** degradation (%) of Rhodamine B dye under various catalyst with different In doped concentrations (120 min)

formation of holes in valence band and electrons excited to conduction band (Eq. 11)

$$ZnO + h\nu \rightarrow ZnO\left(e_{CB} + h_{VB}\right) \tag{11}$$
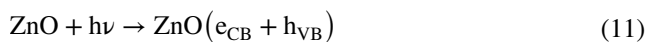
Further, Indium doping results in the formation of trap levels between the valence and conduction band of ZnO. These trap levels effectively red-shift the band edge absorption threshold. Besides the separation of electron–hole pairs process, electron- and hole-driven photoredox reaction lead to the generation of highly active hydroxyl (OH·) radical (Eq. 13) which is mainly responsible for degradation of organic dyes [57]. This is due to the oxygen vacancy defects (V_O^+) and In-doped NPs on the surface of ZnO act as a sink in improving the photogenerated electron–hole pair separation [58]. Also, the photoelectron can be easily trapped by electronic acceptors like adsorbed O_2, to produce a superoxide radical anion ($O\cdot_2^-$)(Eq. 17), whereas the photoinduced holes can be easily trapped by electronic donors, such as organic pollutants, to further oxidation of organic pollutants as described in (Eq. 15). At the short instance electrons and holes oxidation–deoxidization with the electron donors or acceptors, the separation effects of photoinduced electrons is high and the photo-generated electrons and holes can be effectively used. The hydroxyl radical and photogenerated holes are extremely strong, non-selective oxidants that lead to degradation of the Indium at the surface of the catalyst (Eqs. 12–18).

$$h^+ + RhB \rightarrow \text{Oxidation of RhB} \tag{12}$$

$$h^+ + H_2O \rightarrow H^+ + OH\bullet \tag{13}$$

$$OH^- + h^+ \rightarrow OH\bullet \tag{14}$$

$$OH\bullet + RhB \rightarrow +\text{degradation products} + CO_2 + H_2O \tag{15}$$

$$In^{3+} + O_2 \rightarrow In^{2+} + O_2 \tag{16}$$

$$e_{CB} + O_2 \rightarrow O\bullet_2^- \tag{17}$$

$$O\bullet_2^- + RhB \text{ degradation products} + CO_2 + H_2O \tag{18}$$

It can be illustrated by Fig. 11b 6% IZ-NPs show a good photocatalytic activity at 120 min in compared to pure and other nanoparticles. Enhancement in photocatalytic activity can be attributed to the band gap narrowing effect due to extra defect created tail states in the vicinity of valence band [59]. This transition within the tail states requires smaller excitation energy as compared to the band gap (3.30 eV) of pure ZnO and therefore results in improved photocatalytic activity.

7.2 Total organic carbon analysis (TOC)

In order to study the mineralization of RhB by the prepared pure ZnO and IZ-NPs, the TOC concentration of aqueous
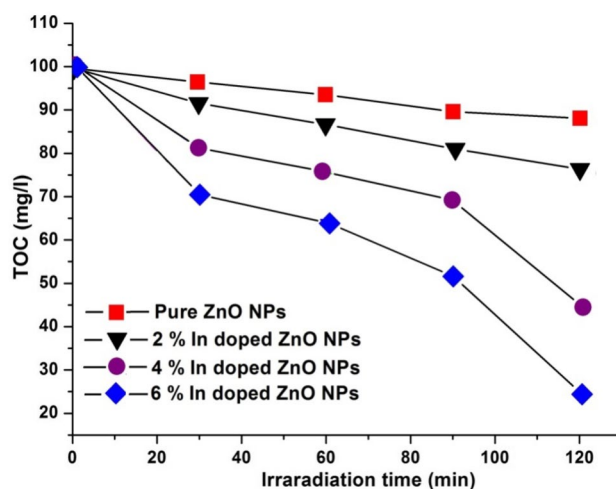
Fig. 11 The effect of irradiation time (TOC) on the photodegradation of RhB of pure and IZ-NPs

RhB solution at different reaction times was analyzed and the results are shown in Fig. 11.

Total organic carbon (TOC) results reveal that 6% In-doped ZnO NPs requires only 120 min to degrade 76% of RhB while pure ZnO shows the TOC of the solution barely changed after the photocatalytic reaction indicating that the photodegradation of RhB molecules occurred to a negligible extent. The results show that RhB solution can be effectively mineralized to CO_2 and H_2O by the prepared IZ-NPs under UV–Vis irradiation. In addition, it also can be seen that pure ZnO nanoparticles showed poor mineralization efficiency compared with Indium doped ZnO nanoparticles. This confirms that IZ-NPs show a good photocatalytic activity than the pure ZnO nanoparticles. Further, it is suggested that the TOC can be eliminated to a larger extent with an increase of time period.

8 Antibacterial studies

Figure 12 displays the zone of inhibition of nanoparticles against the Bacterial *S. aureus* and *S. epidermidis*. From the Fig, it is observed that all the samples show the effective bacterial opposing behavior. This indicates that the dimensionality of nanomaterials can immensely influence the antibacterial activity. Since the different surface-interface characteristics might have different chemical–physical adsorption–desorption abilities towards the bacteria, ensuring in different antibacterial activities [60].

The zones of inhibition measured are listed in Table 4. From Table 4 it is observed that interaction between the nanoparticles and the cell wall of bacteria perish the fact that the growth of *S. aureus* and *S. epidermidis* was more effectively affected by In-doped ZnO nanostructures than
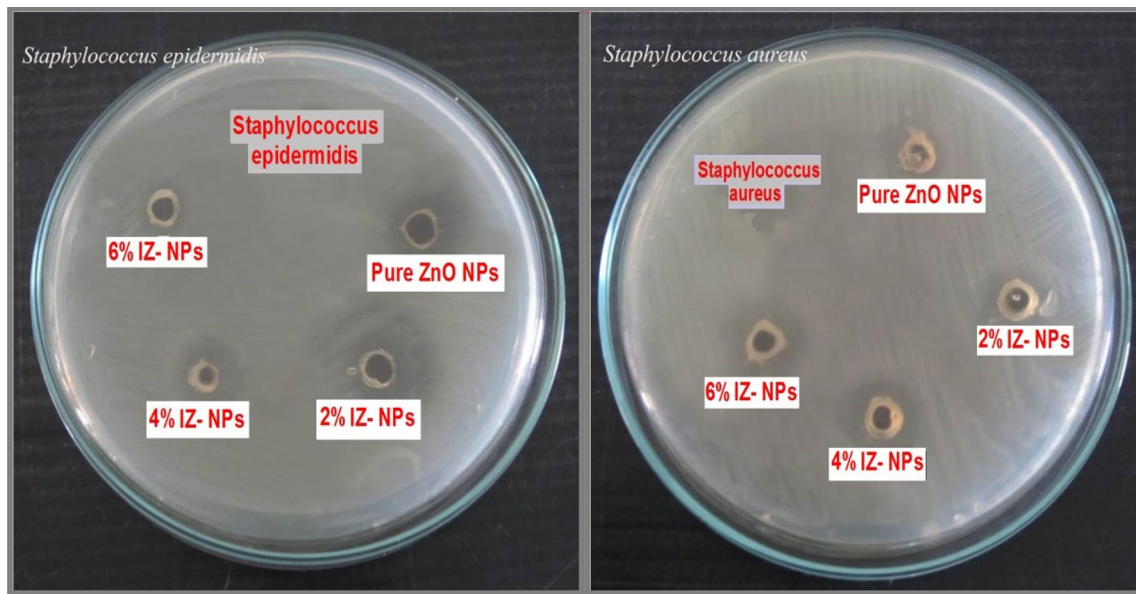
Fig. 12 Zones of Inhibition of ZnO and In-doped ZnO nanoparticles against the given bacteria

that pure ZnO NPs. However, it is noteworthy to mention that *S. aureus* was affected more in compared to *S. epidermidis*. This is due to interaction between nanoparticles and bacteria in the production of increased levels of reactive oxygen species (ROS), mostly hydroxyl radicals (OH) and singlet oxygen [61, 62] and the other is the deposition of the nanoparticles on the surface of bacteria or accumulation of nanoparticles either in the cytoplasm or in the periplasmic region causing disruption of cellular function or disruption and disorganization of membranes [63]. Similar such observations were obtained by Pavithra et al. for the "Effect of In doping on the properties and antibacterial activity of ZnO films prepared by spray pyrolysis" These doped ZnO nanoparticles will be a promising material for a potential drug delivery to cure some very important infections in near future.

9 Conclusion

Pure and IZ-NPs were successfully synthesized by co-precipitation method. XRD results confirm the hexagonal Wurtzite structure of doped ZnO lattice with no any manifestation of the secondary phase. The existence of Indium ions caused a small change in its various lattice parameters. The average crystallite size was reduced from 51 to 28 nm. SEM images also show that the distribution of ZnO nanoparticles improves and crystals size is reduced. The absorption edge slightly shifted towards the longer wavelengths and energy band gap (E_g) has found to decrease with the increase of Indium concentration (3.34–3.17 eV). PL spectrum shows the defect states encountered a series of enhanced visible emissions for the doped NPs. Kinetic evaluation of photocatalytic mechanism on RhB dye has pronounced the degradation rate has increased with the higher In-doped sample. Owing to the more surface area in nanoparticles and the new trapped centers related to doping, the Indium-doped ZnO nanoparticles are more photoactive than pure ZnO. Therefore the synthesized samples showed incredibly intense blue-violet PL emission and also high photocatalytic action under visible irradiations, which is essential for optical devices and organic pollutant related applications as well. Further, the prepared nanoparticles exhibit effective antibacterial activity against *S. aureus* and *S. epidermidis* and can easily inhibit the bacterial growth at the concentration of 0.1%/l. These results suggest pure and doped ZnO nanoparticles have a potential application as a bacteriostatic agent and may have future applications in the development of derivative agents to control the spread and infection of a variety of

Table 4 Average diameter values of zones of inhibition (ZOI) for pure and indium doped ZnO nanoparticles (2–6%)

Bacterial culture	Zones of inhibition (ZOI) in mm			
	ZnO	2% In-ZnO NPs	4% In-ZnO NPs	6% In-ZnO NPs
Pseudomonas	13±0.7	16±0.3	17±0.4	20±0.2
Staphylococcus epidermidis	14±0.4	11±0.3	15±0.5	19±0.2

bacterial strains. Use of doped ZnO-NPs for delivery of antimicrobial or drug molecules will be at its helm in near future.

References

1. P.K. Sharma, M. Kumar, A.C. Pandey, Green luminescent ZnO:Cu^{2}+ nanoparticles for their applications in white-light generation from UV LEDs. J. Nanocryst. Res. **13**, 1629–1637 (2010)
2. Y. Zhang, M.K. Ram, E.K. Stefanakos, D. Yogi Goswami, Synthesis, characterization, and applications of ZnO nanowires. J. Nanomater. **2012**, 1–22, (2012)
3. S.B. Rana, P. Singh, A.K. Sharma, A.W. Carbonari, R. Dogra, Synthesis and characterization of pure and doped ZnO nanoparticles. J. Optoelectron. Adv. Mater. **12**, 257–261 (2010)
4. N. El-Atab, A. Nayfeh, Ultra-small ZnO nanoparticles for charge storage in MOS-memory devices. ECS Trans. **72**, 73–79, (2016)
5. M. Willander, O. Nur, J.R. Sadaf, M.I. Qadir, S. Zaman, A. Zainelabdin, N. Bano, I. Hussain, Luminescence from zinc oxide nanostructures and polymers and their hybrid devices. Materials **3**, 2643–2667 (2010)
6. P.K. Sharma, M. Kumar, A.C. Pandey, Green luminescent ZnO:Cu^{2+} nanoparticles for their applications in white-light generation from UV LEDs. J. Nanopart. Res. **13**, 1629–1637 (2011)
7. L. Zhang, Y. Ding, M. Povey, D. York, ZnO nanofluids: a potential antibacterial agent. Prog. Nat. Sci. **18**, 939–944 (2008)
8. H.S. Hassan, A.B. Kashyout, I. Morsi, A.A.A. Nasser, I. Ali, Synthesis, characterization and fabrication of gas sensor devices using ZnO and ZnO:In nano materials. J. Basic Appl. Sci. **3**, 216–221 (2014)
9. C. Tian, Q. Zhang, A. Wu, M. Jiang, Z. Liang, B. Jiang, H. Fu, Cost-effective large-scale synthesis of ZnO photocatalyst with excellent performance for dye photo degradation. Chem. Commun. (Camb) **48**, 2858–2860 (2012)
10. S. Kuriakose, V. Choudhary, B. Satpati, S. Mohapatra, Structural, optical, and magnetic properties of Ni. Beilstein J. Nanotechnol. **5**, 639–650 (2014)
11. P. Rathore, A.K. Chittora, R. Ameta, S. Sharma, Enhancement of photocatalytic activity of zinc oxide by doping with nitrogen. Sci. Revs. Chem. Commun. **5**, 113–124 (2015)
12. A.H. Abdullah, L.K. Mun, Z. Zainal, M.Z. Hussein, Photodegradation of chlorophenoxyacetic acids by ZnO/γ–Fe$_2$O$_3$ nanocatalysts: a comparative study. Int. J. Chem. **5**, 56–65 (2013)
13. S. Baruah, M.A. Mahmood, M.T.Z. Myint, T. Bora, J. Dutta, Enhanced visible light photocatalysis through fast crystallization of zinc oxide nanorods. Beilstein J. Nanotechnol. **1**, 14–20 (2010)
14. M.T. Uddin, Y. Nicolas, C. Olivier, L. Servant, T. Toupance, S. Li, A. Klein, W. Jaegermann, Improved photocatalytic activity in RuO$_2$–ZnO nanoparticulate heterostructures due to inhomogeneous space charge effects. Phys. Chem. Chem. Phys. **17**, 5090–5102 (2015)
15. R. Yousefi, F. Jamali-Sheini, M. Cheraghizade, S. Khosravi-Gandomani, A. Sáaedi, N.M. Huang, W.J. Basirun, M. Azarang, Enhanced visible-light photocatalytic activity of strontium-doped zinc oxide nanoparticles. Mater. Sci. Semicond. Process. **32**, 152–159 (2015)
16. Y.-M. Hao, S.-Y. Lou, S.-M. Zhou, R.-J. Yuan, G.-Y. Zhu, N. Li, Structural, optical, and magnetic studies of manganese-doped zinc oxide hierarchical microspheres by self-assembly of nanoparticles. Nanoscale Res. Lett. **7**(100), 1–9 (2012)
17. S. Girish Kumar, K.S.R. Koteswara Rao, Zinc oxide based photocatalysis: tailoring surface-bulk structure and related
18. interfacial charge carrier dynamics for better environmental applications. RSC Adv. **5**, 3306–3351 (2015)
18. S. Baruah, S.K. Pal, J. Dutta, Nanostructured zinc oxide for water treatment. Nanosci. Nanotechnol. 2, 90–102 (2012)
19. S. Kuriakose, B. Satpati, S. Mohapatra, Enhanced photocatalytic activity of Co doped ZnO nanodisks and nanorods prepared by a facile wet chemical method. Phys. Chem. Chem. Phys. **16**, 12741–12749 (2014)
20. H. Yamada, K. Suzuki, S. Koizumi, Gene expression profile in human cells exposed to zinc. J. Toxicol. Sci. **32**, 193–196 (2007)
21. Y. Fan, R. Liu, W. Du, Q. Lu, H. Pang, F. Gao, Synthesis of copper(II) Co-ordination polymers and conversion into CuO nanostructures with good photocatalytic, antibacterial and lithium ions better performances. J. Mater. Chem. **22**, 12609–12617 (2012)
22. U. Ozgur, H. Morkoc, *Zinc Oxide: Fundamentals, Materials and Device Technology*. (Wiley, New York, 2009), p. 365
23. H.R. Ghaffarian, M. Saiedi, M.A. Sayyadnejad, Synthesis of ZnO nanoparticles by spray pyrolysis method, Iran. J. Chem. Chem. Eng **30**, 1–6 (2011)
24. C.-C. Lin, Y.-Y. Li, Synthesis of ZnO nanowires by thermal decomposition of zinc acetate dihydrate. Mater. Chem. Phys. **113**, 334–337 (2015)
25. E. Maryanti, D. Damayanti, I. Gustian, S. Salprima Yudha, Synthesis of ZnO nanoparticles by hydrothermal method in aqueous rinds extracts of Sapindus rarak DC. Mater. Lett. **118**, 96–98 (2014)
26. R.M. Alwan, Q.A. Kadhim, K.M. Sahan, R.A. Ali, R.J. Mahdi, N.A. Kassim, A.N. Jassim, Synthesis of zinc oxide nanoparticles via sol–gel route and their characterization. Appl. Surf. Sci. **5**, 1–6 (2015)
27. Arun Vasudevan, Soyoun Jung, Taeksoo Ji, Synthesis and characterization of hydrolysis grown zinc oxide nanorods. ISRN Nanotechnol **2017**, 1–7 (2011). doi:10.5402/2011/983181
28. J. Lang, J. Wang, Q. Zhang, X. Li, Q. Han, M. Wei, Y. Sui, D. Wang, J. Yang, Chemical precipitation synthesis and significant enhancement in photocatalytic activity of Ce-doped ZnO nanoparticles. Ceram. Int. **42**, 14175–14181 (2016)
29. V. Anand, V.C. Srivastav, Zinc oxide nanoparticles synthesis by electrochemical method: optimization of parameters for maximization of productivity and characterization. J. Alloys Compd. **636**, 288–292 (2015)
30. A. Bagabas, A. Alshammari, M.F.A. Aboud, H. Kosslick, Room-temperature synthesis of zinc oxide nanoparticles in different media and their application in cyanide photodegradation. Nanoscale Res. Lett. **8**(516), 1–10 (2013)
31. K. Pradeev raj, K. Sadaiyandi, A. Kennedy, R. Thamizselvi, Structural, optical, photoluminescence and photocatalytic assessment of Sr-doped ZnO nanoparticles. Mater. Chem. Phys. (2016). doi:10.1016/j.matchemphys.2016.07.068
32. Z. Chen, S. Li, Y. Tian, S. Wu, W. Zhang, Sythesis of magnesium oxide doped ZnO nanostructures using electrochemical deposition. Int. J. Electrochem. Sci. **7**, 10620–10626 (2012)
33. M. Schwartz, *Smart Materials*. (CRC Press, Boca Raton, 2008), pp. 1–3
34. S. Talam, S. Rao Karumuri, N. Gunnam, Synthesis, characterization, and spectroscopic properties of ZnO nanoparticles. ISRN Nanotechnol. **2012**, 1–6 (2012)
35. P. Geetha Devi, A. Sakthi Velu, Synthesis, structural and optical properties of pure ZnO and Co doped ZnO nanoparticles prepared by the co-precipitation method. J. Theor. Appl. Phys. (2016). doi:10.1007/s40094-016-0221-0
36. A. Singh, H.L. Vishwakarma, Study of structural, morphological, optical and electroluminescent properties of undoped ZnO nanorods grown by a simple chemical precipitation. Mater. Sci. Poland **33**, 751–759 (2015)

37. T.A. Abdel-Baset, Y.-W. Fang, B. Anis, C.-G. Duan, M. Abdel-Hafiez, Structural and magnetic properties of transition-metal-doped Zn1 – xFexO. Nanoscale Res. Lett., **11**(115), 1–12 (2016)

38. P. Bindu, S. Thomas, Estimation of lattice strain in ZnO nanoparticles: X-ray peak profile analysis. J. Theor. Appl. Phys. **8**, 123–134 (2014)

39. G. Pavithra, M. Bououdina, S. Dhanapandian, P. Dhamodharan, C. Manoharan, Characterization and study of antibacterial activity of spray pyrolysed ZnO:Al thin films. Appl Nanosci. **6**, 815–825 (2016)

40. A. Khorsand Zak, W.H.A. Majid, M.E. Abrishami, R. Yousefi, X-ray analysis of ZnO nanoparticles by Williamsone Hall and size strain plot methods. Solid State Sci. **13**, 251–256

41. S. Kumari, P. Kumar, M. Kar, L. Kumar, V. Kumar, Structural analysis by rietveld method and its correlation with optical propertis of nanocrystalline zinc oxide. Adv. Mater. Lett. **6**, 139–147

42. V. Sesha Sai Kumar, K. Venkateswara Rao, X-ray peak broadening analysis and optical studies of ZnO nanoparticles derived by surfactant assisted combustion synthesis. J. Nano Electron. Phys. **5**, 02026–02026 (2013)

43. S. Mohan, K.S. Thind, G. Sharma, Effect of Nd^{3+} concentration on the physical and absorption properties of sodium-lead-borate glasses. Braz. J. Phys. **37**, 1306–1313 (2007)

44. K. N'Konou, M. Haris, Y. Lare, M. Baneto, K. Napo, Effect of barium doping on the physical properties of zinc oxide nanoparticles elaborated via sonochemical synthesis method. Pramana **87**, 1–7 (2016)

45. D.K. Sharma, K.K. Sharma, V. Kumar, A. Sharma, Effect of Ce doping on the structural, optical and magnetic properties of ZnO nanoparticles. J. Mater. Sci. (2016). doi:10.1007/s10854-016-5117-x

46. P. Kaur, S. Kumar, N.S. Negi, S.M. Rao, Enhanced magnetism in Cr-doped ZnO nanoparticles with nitrogen co-doping synthesized using sol–gel technique. Appl. Nanosci. **5**, 367–372 (2015)

47. B.H. Soni, M.P. Deshpande, S.V. Bhatt, N. Garg, N.N. Pandya, S.H. Chaki, Influence of Mn doping on optical properties of ZnO nanoparticles synthesized by microwave irradiation. J. Opt. **42**, 328–334 (2013)

48. V. Etacheri, R. Roshan, V. Kumar, Mg-doped ZnO nanoparticles for efficient sunlight-driven photocatalysis. ACS Appl. Mater. Interfaces **4**, 2717–2725 (2012)

49. C.H. Venkata Reddy, B. Babu, S.V. Prabhakar Vattikuti, R.V.S.S.N. Ravikumar, J. Shim, Structural and optical properties of vanadium doped SnO_2 Nanoparticles with high photocatalytic activities. J. Lumin. **179**, 26–34 (2016)

50. R. Elilarassi, G. Chandrasekaran, Influence of Co-doping on the structural, optical and magnetic properties of ZnO nanoparticles synthesized using auto-combustion method. J. Mater. Sci. **24**, 96–105 (2012)

51. V. Ganasan, C. Sudarsanakumar, V.P. Radhakrishna Prabhu, R. Mahadevan, Sreeja Sreedharan, Highly transparent and luminescent nanostructured Eu_2O_3. In *2nd international conference on structural nano composites (NANOSTRUC 2014)*, Madrid, Spain, pp. 1–6 (2014)

52. D. Sarkar, P.K. Giri Bappaditya Pal, Structural, optical, and magnetic properties of Ni. Appl. Surf. Sci. **356**, 804–811 (2015)

53. S. Ahmed, M.G. Rasul, W.N. Martens, R. Brown, M.A. Hashib, Heterogeneous photocatalytic degradation of phenols in wastewater: a review on current status and developments. Desalination **261**, 3–18 (2010)

54. P. HemalathaS. N. Karthick, K.V. Hemalatha, M. Yi, H.-J. Kim, M. Alagar, La-doped ZnO nanoflower as photocatalyst for methylene blue dye degradation under UV irradiation. J. Mater. Sci. **27**, 2367–2378 (2015)

55. Z. Barzgari, A. Ghazizadeh, S.Z. Askari, Preparation of Mn-doped ZnO nanostructured for photocatalytic degradation of orange G under solar light. Res. Chem. Intermed. **42**, 84303–84315 (2015)

56. K.M. Lee, C.W. Lai, K.S. Ngai, J.C. Juan, Recent developments of zinc oxide based photocatalyst in watertreatment technology: a review. Water Res. **88**, 428–448 (2016)

57. J. Zhong, J. Li, X.Y. He, J. Zeng, Y. Lu, W. Hu, K. Lin, Improved photocatalytic performance of Pd-doped ZnO. Curr. Appl. Phys. **12**, 998–1001 (2012)

58. T. Bhuyan, M. Khanuja, R. Sharma, S. Patel, M.R. Reddy, S. Anand, A. Varma, A Comparative study of pure and copper (CU) doped ZnO nanorods for antibacterial AND photocatalytic applications with their mechanism of action. J. Nanopart. Res. **17**, 1–11 (2015)

59. I.Y.-Y. Bu, Enhanced photocatalytic activity of sol–gel derived ZnO via the co-doping process. Superlattices Microstruct. **86**, 36–42 (2015)

60. H. Zhang, D.R. Yang, Y.J. Ji, X.Y. Ma, J. Xu, D.L. Que, Low temperature synthesis of flowerlike ZnO nanostructures by cetyltri methyl ammonium bromide-assisted hydrothermal process. J. Phys. Chem. B. **108**, 3955–3958 (2004)

61. R. Brayner, R. Ferrari-Iliou, N. Brivois, S. Djediat, M.F. Benedetti, F. Fievet, Toxicological impact studies based on *Escherichia coli* bacteria in ultrafine ZnO nanoparticles colloidal medium. Nano Lett. **6**, 866–870 (2006)

62. L. Zhang, Y. Jiang, Y. Ding, M. Povey, D. York, Investigation into the antibacterial behaviour of suspensions of ZnO nanoparticles (ZnO nanofluids). J. Nanopart. Res. **9**, 479–489 (2007)

63. S. Sonia, N.D. Jayram, P. Suresh Kumar, D. Mangalaraj, N. Ponpandian, C. Viswanathan, Effect of NaOH concentration on structural, surface and antibacterial activity of CuO nanorods synthesized by direct sonochemical method. Superlattices Microstruct. **66**, 1–9 (2014)